NASA TECHNICAL MEMORANDUM 102598
AVSCOM TECHNICAL MEMORANDUM 90-B-001

FATIGUE CRACK INITIATION AND SMALL CRACK GROWTH IN SEVERAL AIRFRAME ALLOYS

M. H. Swain, J. C. Newman, Jr., E. P. Phillips, and R. A. Everett, Jr.

January 1990

National Aeronautics and Space Administration

Langley Research Center
Hampton, Virginia 23665

US ARMY AVIATION SYSTEMS COMMAND
AVIATION R&T ACTIVITY

FATIGUE CRACK INITIATION AND SMALL CRACK GROWTH IN SEVERAL AIRFRAME ALLOYS

M.H. Swain*, J.C. Newman, Jr.** , E.P. Phillips**, R.A. Everett***

The growth of naturally-initiated small cracks under a variety of constant amplitude and variable amplitude load sequences is examined for several airframe materials: the conventional aluminum alloys, 2024-T3 and 7075-T6, the aluminum-lithium alloy, 2090-T8E41, and 4340 steel. Loading conditions investigated include constant amplitude loading at R = 0.5, 0, -1 and -2 and the variable amplitude sequences FALSTAFF, Mini-TWIST, and FELIX/28. Crack growth was measured at the root of semicircular edge notches using acetate replicas. Crack growth rates are compared, on a stress intensity factor range basis, to those for large cracks to evaluate the extent of the small crack effect in each alloy. In addition, the various alloys are compared on a crack initiation and crack growth morphology basis.

INTRODUCTION

Over the past decade numerous researchers (1-4) have observed that the growth characteristics of small cracks (less than about one millimeter in length) differ from those of large cracks in the same material. On the basis of linear elastic fracture mechanics, the small cracks were found to grow much faster than would be predicted from large crack data and to grow at stress intensity factor levels well below the threshold for large cracks. Because crack growth from small microstructural defects (.002 - .020 mm) at fastener holes and fillets in airframe structures can consume a major portion of the component's fatigue life, it is desirable to incorporate this regime of crack growth behavior into airframe design procedures. Currently there are two approaches to fatigue life prediction - (1) the damage tolerant and durability concepts which assume an initial crack exists in a new structure and relies on crack propagation to establish inspection intervals and (2) the safe-life approach which relies on "crack initiation" data to establish total fatigue life. The small-crack data bases which have been developed seem to indicate that for a wide variety of materials and loading, fatigue life is primarily crack propagation from a material "defect" particle. Thus the crack growth prediction methodologies which are being developed may be useful to predict total fatigue life. Before this philosophy can be generally applied, one must develop insight into the small-crack growth behaviors that might occur as a function of microstructure, constituent-particle population and applied load sequence, as well as determine whether or not these behaviors can be correlated with a standard crack growth driving force, such as Mode I stress intensity factor range.

*Lockheed Engineering & Sciences Co., Hampton, VA 23666, **NASA Langley Research Center, Hampton, VA 23665, ***Army Aerostructures Directorate, NASA Langley Research Center, Hampton, VA 23665

MATERIAL AND EXPERIMENTAL PROCEDURES

Materials investigated included 2024-T3, 7075-T6, 2090-T8E41 and 4340 steel (quenched and tempered to a hardness of 45 Rockwell C). Table 1 gives the tensile properties and microstructural parameters for each alloy. Both 2024 and 7075 have the typical pancake microstructure of rolled sheet, but the 7075 grains are smaller. The 2090 subgrain structure is visible optically because the subgrain boundaries are decorated with Al_2CuLi (T_1 precipitates). Texture analysis performed by Bowen(4) shows a deformation texture and, therefore, an un-recrystallized condition. Each aluminum alloy contains a distribution of Fe-rich constituent particles approximately 5 x 15 μm. The 4340 microstructure is tempered martensite; the constituent particles are calcium aluminate (10-30 μm) or manganese sulfide stringers (5 x 10-60 μm).

TABLE 1 - Average Tensile Properties and Microstructural Parameters.

Material	Thickness B, mm	σ_u MPa	σ_y(.2%) MPa	Typical Grain Size (mm) L	T	S	
2024-T3	2.3	495	355	.100	.050	.025	*subgrain size
7075-T6	2.3	575	520	.030	.025	.010	**prior
2090-T8E41	2.15	580	525	.010*	.005*	.005*	austenite
4340 Steel	5.1	1500	1410	.010**	.010**	.010**	grain size

Single edge notched tensile (SENT) specimens, with notch radius of 3.18 mm, were machined with the loading axis parallel to the rolling direction of the sheet. Aluminum specimens were 50 mm wide and steel specimens were 25 mm, yielding notch stress concentration factors of 3.15 and 3.30, respectively. Aluminum specimens were chemically polished and steel specimens heat treated and electropolished prior to testing. Each alloy was tested under at least two constant amplitude loading conditions and one of the following variable amplitude load spectra: FALSTAFF(2024), wing of a fighter aircraft; Mini-TWIST(7075, 2090), wing of a transport aircraft; or FELIX/28(4340), 'fixed' or semi-rigid rotor of a helicopter. Crack length measurements were obtained from acetate replicas of the notch root taken at cyclic intervals during the test. Surface crack length, 2a, or corner crack length, a, was measured as the projection of the crack onto a plane normal to the loading axis. Crack depth below the notch surface is c. Crack shape relationships (c/a vs a) for each alloy were obtained from specimens which were cycled until a surface crack had grown partially across the bore of the notch and then pulled in tension to failure. Growth of surface cracks and corner cracks emanating from a semicircular edge notch was analyzed using Mode I stress intensity factor equations developed by Newman(3) and presented for this specimen geometry by Swain, et. al., (4). A value of stress intensity factor range, ΔK, was calculated for the average crack length between measurements taken from consecutive replicas. The ΔK values for the variable amplitude loading were defined from the maximum and minimum stress in the entire spectrum.

RESULTS AND DISCUSSION

The growth of small cracks across the notch surface was monitored beginning with cracks as small as 5-10 μm up to lengths of more than 2000 μm (2 mm). Except for a few corner cracks, crack initiation occurred along the bore of the notch at a constituent particle or a pit resulting from the removal of a particle during machining or polishing. Figure 1 shows a replica of a typical small crack in 7075 which initiated

at a constituent particle site. The fracture surface of this specimen shows the initiation site to be a cluster of Fe-rich inclusions. The fracture surface is transgranular, and, although the crack orientation may vary from one grain to the next, the overall fracture surface is normal to the load axis. Crack initiation at Fe-rich particles, approximately 5 μm x 10 μm, is typical of all three aluminum alloys. In 2024, crack growth is also transgranular and normal to the load axis for all loading conditions.

The aluminum lithium alloy exhibits a unique crack growth behavior under constant amplitude loading at both R = 0 and -1. The plane of crack growth once it extends beyond the inclusion particle is oriented about 35° to the load axis, as shown in Figure 2, for both a small crack and that same crack as it approaches the full width of the notch. The crack will sometimes bifurcate, but the new crack plane is also at 35°. Yoder (6) has shown highly angled fracture paths for compact specimens of 2090 and attributed the behavior to both the presence of lithium, which increases the tendency for planar slip, and the development of a strong texture during processing. The steeply angled crack segments reported in reference 4 were on the order of 100 μm, producing a rough, furrowed surface thought to be beneficial to fatigue crack growth resistance. The SENT specimen fracture surface, however, contained angled crack segments approximately 1000 μm in length (Fig. 2). The coarse scale of this fracture surface roughness may not be effective in reducing crack growth rates.

The highly angled crack growth in 2090 was suppressed under the variable amplitude load spectrum, Mini-TWIST. Surface cracks initiated at inclusion particles, grew for 70-120 μm at an angle of 35° and then grew normal to the load axis. Figure 3 shows a comparison of the crack profile along the notch surface for 2090 specimens tested under R = -1 and Mini-TWIST loading. However, spectrum results by Blom(4) for SENT specimens from this 2090 sheet indicate growth normal to the load axis for the full TWIST spectrum but angled growth for FALSTAFF; while tests conducted by Cook (4) using FELIX indicated that normal growth was promoted at low Smax and angled growth for high Smax. The Mini-TWIST tests in the current work were conducted at levels of Smax above which angled crack growth occurred for FELIX. The crack growth morphology is apparently highly dependent on the characteristics of the individual spectrum as well as stress level.

For 4340 steel, cracks also initiated at constituent particle sites. Most cracks initiated at sites associated with calcium aluminate particles, and only occasionally with MnS particles. Initiation at MnS particles was not observed by Lankford(7), but he used smooth specimens thereby increasing the probability that a large calcium aluminate particle was present at the gage section surface. Figure 4 shows calcium aluminate sites to be the 'preferred' initiation sites, producing lives under the Felix/28 spectrum which were shorter than for MnS initiated cracks. The runout data suggest that no sizeable constituent particle of either type was present along the notch root.

The crack growth rates for SENT specimens were compared to those for large cracks for middle-crack tension (MT) specimens manufactured from the same alloy sheets. Figure 5(a) shows a comparison between small and large crack growth rate data for 2024-T3 tested under constant amplitude loading at R = -1. The small cracks grew at stress intensity factor range values, ΔK, well below the large crack threshold, ΔK_{th}, of 6 MPa$\sqrt{m}$. There appears to be a stress level effect, in that, for a given ΔK, cracks growing under higher levels of Smax grew at higher rates. Above the large crack threshold, small crack growth continues at faster rates, blending into the large crack data for ΔK above approximately 15 MPa$\sqrt{m}$. At all R values all the aluminum

alloys exhibited crack growth below ΔK_{th}. Above ΔK_{th}, small cracks grew faster than large cracks for $R \leq 0$. For 4340 steel, growth below ΔK_{th} was observed only for R = -1, and above ΔK_{th} small and large crack growth rates agreed. Table 2 shows a comparison of large and small crack growth characteristics for each alloy.

TABLE 2 - Characteristics of Small Versus Large Crack Growth Rates.

Loading	Materials Tested	Growth Below ΔK_{th}	Stress Level Effect	Faster Growth Above ΔK_{th}	KEY
R = -2	2	2	2	2	2 - 2024-T3
R = -1	2-7-L-4	2-7-L-4	2	2-7-L	7 - 7075-T6
R = 0	2-7-L-4	2-7-L	2	2-7-L	L - 2090-T8E41
R = 0.5	2-7-4	2-7	-	-	4 - 4340 Steel

The 2090-T8E41 alloy was developed with 7075-T6 as a target for mechanical properties (see Table 1). It is of interest, therefore to compare the fatigue crack growth rates for both large and small cracks for these two alloys. Figure 5(b) shows crack growth data for R = -1. The large crack 2090 data for this sheet was reported by Mazur and Rudd (4). For large cracks, the crack growth rate for 2090 is lower than that for 7075 for ΔK greater than 10 MPa$\sqrt{m}$ and nearly equal for ΔK down to threshold. The threshold for 2090 is only slightly higher at 4.5 MPa$\sqrt{m}$ compared to 3.8 MPa$\sqrt{m}$ for 7075. A comparison of small crack data for these two alloys, shows no difference in crack growth rates for ΔK up to 10 MPa$\sqrt{m}$ and a separation in rates above that level which follows the trend of the large crack data. The agreement of 2090 and 7075 small-crack data for low values of ΔK indicates that angled growth producing coarse surface roughness is not effective in reducing crack growth rates. This correlation was found using a Mode I analysis which measures only the component of crack length which is normal to the loading axis. Under the Mini-TWIST spectrum, where crack growth for small cracks was normal to the loading axis, there is also good agreement between 2090 and 7075(Figure 5(c)).

CONCLUSIONS

For 2024-T3, 7075-T6, 2090-T8E41 and 4340 steel (45 Rc) for constant amplitude loading and several variable amplitude load spectra: (1) Crack initiation occurred primarily at constituent particle sites whose average size varied from 5-15 μm. (2) Small cracks grew below the large crack threshold for all loading types in aluminum alloys but only for R = -1 loading in 4340 steel. (3) In 2090, small cracks grew at 35° to the load axis for R = 0 and -1 and normal to the load axis for Mini-TWIST. (4) Good agreement was found between 2090 and 7075 crack growth rates for all loading types using the crack length projected on a plane normal to the load axis.

REFERENCES

(1) Pearson, S., Engng. Fract. Mech., Vol. 7, No. 2, 1975, pp. 235-247.
(2) Ritchie, R.O., and Lankford, J., Small Fatigue Cracks, The Met .Soc., 1986.
(3) Newman, J.C., Jr., and Edwards, P.R., AGARD Rep. No. 732, 1988.
(4) AGARD Rep. No.767 (11 individual papers, authors cited in text), 1990.
(5) Swain, M.H., and Newman, J.C., Jr., AGARD CP-376, 1984, pp. 12.1-12.17.
(6) Yoder, G.R., Pao, M.A., and Imam, M.A., and Cooley, L.A., 5th Intl. Al-Li Conf., Sanders, T.H., and Starke, E.A., Jr., eds, Vol. 2, 1989, pp. 1033-1041.
(7) Lankford, J., Engng Fract. Mech., Vol. 9, No. 3, 1977, pp.617-624.

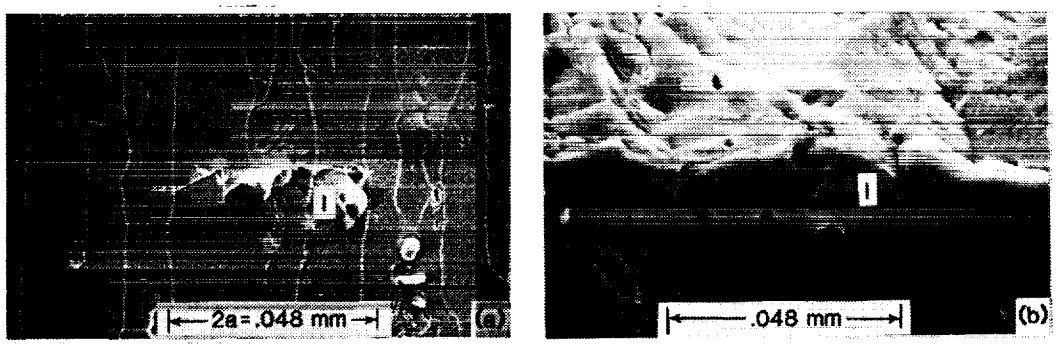

Figure 1. (a) Replica of small crack and (b) fracture surface showing inclusion particle cluster at crack initiation site in 7075-T6.

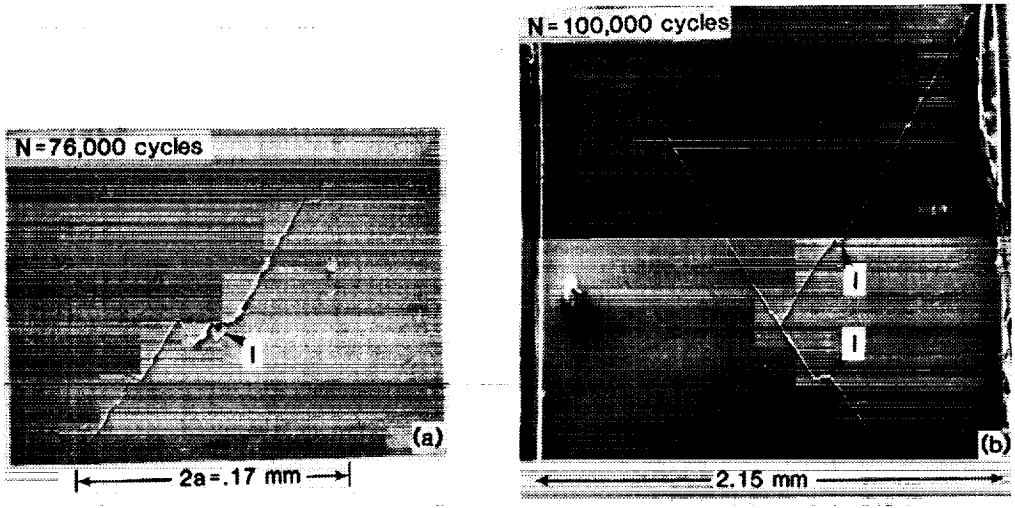

Figure 2. Replica of (a) small crack at inclusion particle site and (b) angled cracks approaching edge of notch in 2090-T8E41.

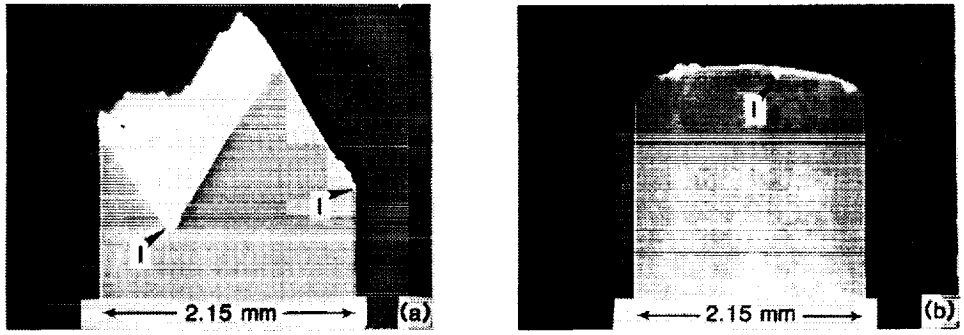

Figure 3. Fracture surface profile of 2090-T8E41 under (a) R = -1 and (b) Mini-TWIST loading.

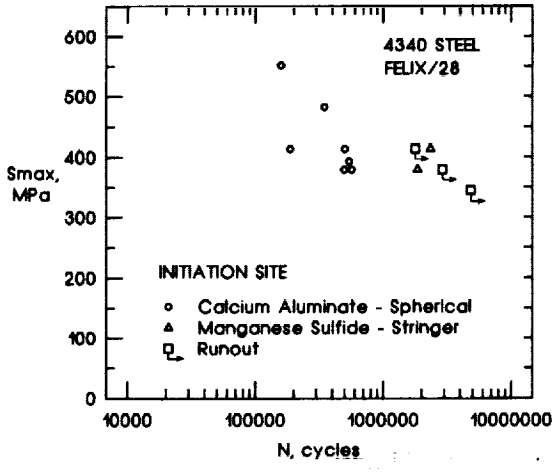

Figure 4. Fatigue life of 4340 steel under FELIX/28.

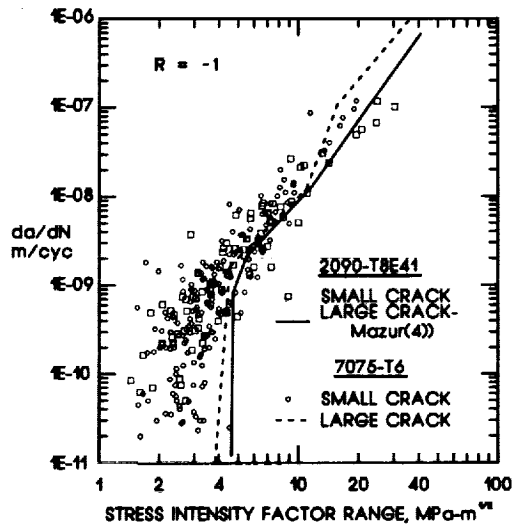

5.(a)

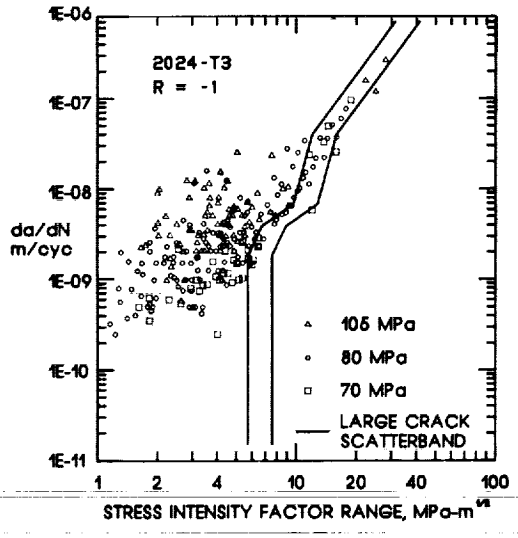

5.(b)

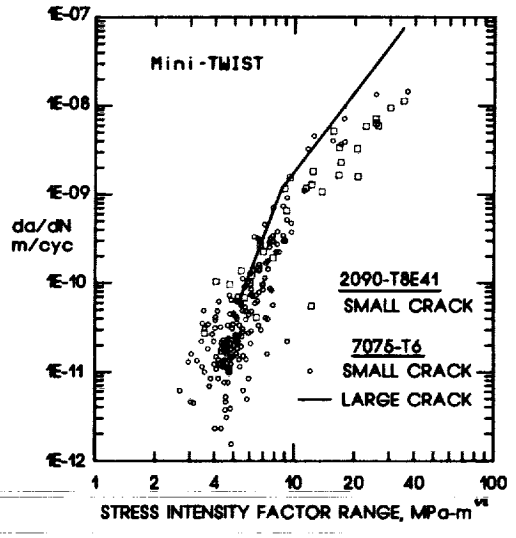

5.(c)

Figure 5. Small and large crack data for (a) 2024-T3 under R = -1, and 2090-T8E41 and 7075-T6 under (b) R = -1 and (c) Mini-TWIST.

NASA
National Aeronautics and Space Administration

Report Documentation Page

1. Report No.	2. Government Accession No.	3. Recipient's Catalog No.
NASA TM-102598 AVSCOM TM-90-B-001		

4. Title and Subtitle

Fatigue Crack Initiation and Small Crack Growth in Several Airframe Alloys

5. Report Date

January 1990

6. Performing Organization Code

7. Author(s)

M. H. Swain*; J. C. Newman, Jr.; E. P. Phillips; R. A. Everett, Jr.**

8. Performing Organization Report No.

10. Work Unit No.

505-63-01-05

9. Performing Organization Name and Address

NASA Langley Research Center, Hampton, VA 23665-5225
U.S. ArmyAviation Research and Technology Activity (AVSCOM)
Aerostructures Directorate
Hampton, VA 23665-5225

11. Contract or Grant No.

13. Type of Report and Period Covered

Technical Memorandum

12. Sponsoring Agency Name and Address

National Aeronautics and Space Administration
Washington, DC 20546-0001
U.S. Army Aviation Systems Command
St. Louis, MO 63166

14. Sponsoring Agency Code

15. Supplementary Notes

*Lockheed Engineering & Sciences Co., Hampton, VA 23666
**U.S. Army Aerostructures Directorate, USAARTA-AVSCOM

16. Abstract

The growth of naturally-initiated small cracks under a variety of constant amplitude and variable amplitude load sequences is examined for several airframe materials: the conventional aluminum alloys, 2024-T3 and 7075-T6, the aluminum-lithium alloy, 2090-T8E41 and 4340 steel. Loading conditions investigated include constant amplitude loading at R = 0.5, 0, -1 and -2 and the variable amplitude sequences FALSTAFF, Mini-TWIST, and FELIX/28. Crack growth was measured at the root of semicircular edge notches using acetate replicas. Crack growth rates are compared, on a stress intensity factor range basis, to those for large cracks to evaluate the extent of the small crack effect in each alloy. In addition, the various alloys are compared on a crack initiation and crack growth morphology basis.

17. Key Words (Suggested by Author(s))	18. Distribution Statement
Fatigue (materials) Steels Crack Initiation Short Cracks Crack Propagation Aluminum Alloys Aluminum Lithium Alloys	Unclassified - Unlimited Subject Category - 39

19. Security Classif. (of this report)	20. Security Classif. (of this page)	21. No. of pages	22. Price
Unclassified	Unclassified	7	A02